



RESEARCH ARTICLE

Open Access



Characteristics of temporal variability of long-duration bursts of high-energy radiation associated with thunderclouds on the Tibetan plateau

Harufumi Tsuchiya^{1*} , Kinya Hibino² , Kazumasa Kawata³, Munehiro Ohnishi³, Masato Takita³, Kazuoki Munakata⁴, Chihiro Kato⁴, Susumu Shimoda⁵, Quanqi Shi⁶, Shuo Wang⁶, Chenyao Han⁶ and Liuming Zhai⁷

Abstract

From 1998 to 2017, neutron monitors located at an altitude of 4300 m on the Tibetan plateau detected 127 long-duration bursts of high-energy radiation in association with thunderclouds. These bursts typically lasted for 10–40 min, and 89% of them occurred between 10:00 and 24:00 local time. They were also found to be more likely to occur at night, especially during 18:00–06:00 local time period. The observed diurnal and seasonal variations in burst frequency were consistent with the frequencies of lightning and precipitation on the Tibetan plateau. Based on 19 years of data, the present study suggests that an annual variation in burst frequency has a periodicity of ~ 16 years and a lag of ~ 3 years relative to solar activity.

Keywords Thunderclouds, Particle acceleration, High-energy radiation, Time variability, Solar activity, Tibetan plateau

1 Introduction

In the 1920s, C. T. R. Wilson proposed that electrons in thunderclouds are accelerated to high energy in strong electric fields and produce X-rays by bremsstrahlung (Wilson 1924, 1925). Since then, many observations have shown that lightning and thunderclouds generate such X-ray signals, confirming that they are indeed powerful particle accelerators (Dwyer et al. 2012, and references therein). Beyond the Wilson prediction, bremsstrahlung gamma rays with a few tens of MeV have been detected from lightning and thunderclouds. The detection of the high-energy photons suggests that lightning and thunderclouds can accelerate electrons beyond a few tens of MeV inside them. Theoretical works (e.g., Gurevich et al. 1992; Dwyer 2003, 2007; Babich et al. 2004, 2010) have pointed out that the production of those high-energy radiations is due to relativistic runaway electrons. Seed electrons produced by, for example, cosmic rays are thought to be

*Correspondence:

Harufumi Tsuchiya
tsuchiya.harufumi@jaea.go.jp

¹ Nuclear Science and Engineering Center, Japan Atomic Energy Agency, 2-4, Shirakata, Tokai-mura, Naka-gun, Ibaraki 319-1195, Japan

² Faculty of Engineering, Kanagawa University, Yokohama, Kanagawa 221-8686, Japan

³ Institute for Cosmic Ray Research, University of the Tokyo, 5-1-5, Kashiwanoha, Kashiwa, Chiba 277-8582, Japan

⁴ Department of Physics, Shinshu University, Matsumoto, Nagano 390-8621, Japan

⁵ RIKEN, 2-1, Hirosawa, Wako, Saitama 351-0198, Japan

⁶ Shandong Provincial Key Laboratory of Optical Astronomy and Solar-Terrestrial Environment, Institute of Space Sciences, School of Space Science and Physics, Shandong University, Weihai 264209, China

⁷ National Astronomical Observatories, Chinese Academy of Sciences, Beijing 100101, China

accelerated to relativistic energies when electric fields exceed a critical threshold and become such runaway electrons.

Solar activity influences the heliospheric magnetic field, resulting in variations in the intensity of galactic cosmic rays reaching the Earth in an approximately 11-year cycle. Therefore, it is thought that solar activity, by affecting the flux of galactic cosmic rays reaching the Earth, also impacts the production of runaway electrons. However, it remains unclear whether cosmic rays or solar activity plays a role in producing the runaway electrons responsible for high-energy bremsstrahlung gamma rays.

Bursts of high-energy radiation during thunderstorms can be categorized into two types when classified simply by their duration. One type is characterized by intense short-duration bursts lasting for microseconds to milliseconds. The other type is a long-duration burst, which lasts from a few seconds to a few tens of minutes and exhibits relatively fainter characteristics compared to the short-duration bursts. Numerous measurements of these short-duration bursts have been taken by space- and ground-based detectors and revealed several characteristics including the source altitude and their relation to lightning. In contrast to short-duration bursts, long-duration bursts such as gamma-ray glows or terrestrial ground enhancements (TGEs) have been observed less frequently until recently. However, observations made in the coastal area of the Japan Sea (Torii et al. 2002; Tsuchiya et al. 2007a, 2011; Wada et al. 2021a), at high mountains (Torii et al. 2009; Tsuchiya et al. 2009; Chilingarian et al. 2010, 2011; Tsuchiya et al. 2012) and at high aircraft altitude (Østgaard et al. 2019; Kochkin et al. 2021) have led to increased detection of these long-duration bursts and have drawn attention to their characteristics, including their duration and their correlation with meteorological phenomena.

The increasing amount of data on long-duration bursts have allowed us to compile a comprehensive catalog of such phenomena and to gain insight into their characteristics at various observation sites, including high mountain regions (Chilingarian et al. 2019) and coastal areas of the Japan Sea (Wada et al. 2021b). However, more data are needed to explore whether there is a correlation between long-duration bursts and cosmic rays and to understand the meteorological and geographical factors that contribute to the generation of these bursts. By studying these conditions, we can identify commonalities among long-duration bursts and develop a deeper understanding of their production mechanisms. To this end, we will present observational results obtained by neutron monitors (NM) at Yangbajing on the Tibetan plateau (TP) during 1998–2017 and then discuss the temporal variability of long-duration bursts.

2 Experiments

2.1 Overview

The Yangbajing NM has been in operation at the Yangbajing cosmic-ray observatory for more than two decades. The observatory is located at an altitude of 4300 m (corresponding to an atmospheric depth of $\sim 600 \text{ g cm}^{-2}$) in the TP. In addition, electric field mills (EFMs) have been deployed at the observatory in 2010 to study possible correlations between variations in count rate measured by a detector such as the Yangbajing NM and electric fields (EFs) (Amenomori et al. 2013). To clarify the points of the present work, we briefly explain their characteristics below.

2.2 Neutron monitor

The main purpose of the Yangbajing NM is to investigate the ion acceleration at the solar surface and to monitor galactic cosmic-ray intensity associated with the solar activity (Miyasaka et al. 2005; Tsuchiya et al. 2007b). In the present study, the NM is repurposed to examine the production mechanism of long-duration bursts of high-energy radiation associated with thunderclouds. Hereafter, the term “long-duration burst” is employed to refer to the high-energy radiation detected by the Yangbajing NM in association with thunderclouds.

As shown in Fig. 1, the Yangbajing NM consists of 28 NM-type BF₃ counters surrounded by lead blocks and polyethylene in the standard NM64 configuration. Each NM unit has one BF₃ counter with dimensions of 190 cm in length and 15 cm in diameter. The total area of the Yangbajing NM is 32 m². The outermost polyethylene serves the purpose of moderating incoming fast neutrons, while the embedded lead blocks breed the moderated neutrons via (n, xn) reactions to enhance the detection efficiency for neutrons (x represents a number). When entering the BF₃ counters, the moderated neutrons undergo the (n, α) reaction: $n + {}^{10}\text{B} \rightarrow \alpha + {}^7\text{Li}$. The cross sections of this reaction become larger as the

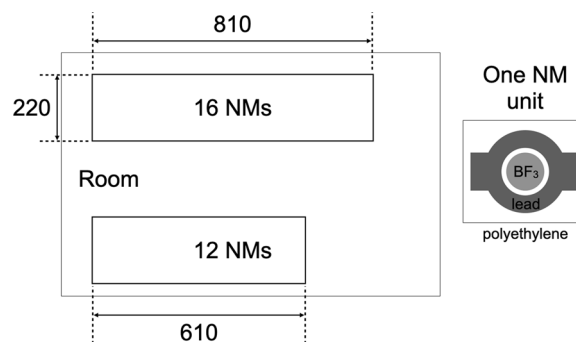


Fig. 1 Arrangement of the Yangbajing NM in a room and a cross-sectional view of one unit, measured in centimeters

neutron energy approaches the thermal energy, thus allowing efficient detection of neutrons in thermal to epithermal energy ranges. To further improve neutron detection efficiency, the isotopic composition of ^{10}B in each BF_3 counter is enriched to 98% from a natural isotopic ratio of $\sim 20\%$. Charged particles produced by the above reactions lose energy due to the ionization loss in gas, resulting in anode signals in the counter. A data acquisition system collects the output signals from each counter and registers the number of signals every one second.

In our previous study (Tsuchiya et al. 2012), we determined the proportions of individual particles that contribute to the total count rate of the Yangbajing NM. Secondary cosmic-ray neutrons and protons dominate the total count rate with fractions of 83 and 12%, respectively. In contrast, leptons, including gamma rays and electrons, contribute to it with only 5% [see also Clem and Dorman (2000)]. The previous study also indicated that the same type of NMs as the Yangbajing NM have a small but non-negligible detection efficiency for gamma rays through photonuclear reactions with lead blocks ($\gamma + {}^A\text{Pb} \rightarrow \text{n} + {}^{A-1}\text{Pb}$) ($A = 206, 207, 208$), with a threshold gamma-ray energy of 7 MeV (IAEA 2000). Given these insights, we demonstrated that bremsstrahlung photons were responsible for the observed count increases during thunderstorms in the Yangbajing NM, rather than neutrons produced by photonuclear reactions in the atmosphere [e.g., Enoto et al. (2017)]. Therefore, for the present study as well, we assume that count increases of the Yangbajing NM can be attributed primarily to bremsstrahlung photons with energy higher than 7 MeV.

2.3 Electric field mill

Electric field data play a crucial role in understanding the association of observed increases with thunderclouds and lightning. For this purpose, two BOLTECK EFM-100 commercial electric field mills have been operational at the observatory since 2010, positioned 25 m apart. One is situated at ground level, while the other is mounted atop an experimental building. The vertical separation between them is approximately 3.4 m. The signals from both EFMs are transmitted to computers within the building via optical cables. These signals are recorded at an interval of every 0.1 s, providing field strength below 100 kV m^{-1} , with a measurement resolution of 20 V m^{-1} .

3 Analysis

To identify long-duration bursts, we performed several steps of analysis of data collected by the Yangbajing NM from 1998 to 2017. First, we made a 5-minute count

history corrected for atmospheric pressure variations for each day. Pressure fluctuations typically induce count changes within $\pm 2\%$. Second, we constructed an occurrence histogram of NM counts in every 5-minute count history, $N_{5\text{min}}$, and fitted a Gaussian function to this histogram to determine the mean value N_{BG} and the standard deviation $\sigma_{1\text{day}}$ of the Gaussian function every day. The resulting $\sigma_{1\text{day}}$ served as an estimate of the uncertainty in the 5-minute counts for each day. Third, we calculated the statistical significance, σ_s , for each $N_{5\text{min}}$ using the formula;

$$\sigma_s = \frac{N_{5\text{min}} - N_{\text{BG}}}{\sqrt{N_{5\text{min}} + \sigma_{1\text{day}}^2}}. \quad (1)$$

This allowed us to assess whether the daily NM data contained count bins with $\sigma_s > 4$. The probability of encountering a bin with a significance of 4 or higher by chance is 5×10^{-5} . Therefore, out of the 288 bins in each 5-minute count history, the number of bins with a significance of 4σ or greater is only 0.014. Among the $N_{5\text{min}}$ counts, we defined the most prominent one as the peak count, N_p , in each 5-minute count history. This data set, which we refer to as the “potential burst set”, contains 135 events that represent possible long-duration bursts associated with thunderclouds.

From the potential data set, we extracted a 5-minute count history over a time span of $\pm 2 \text{ h}$ centered on the peak time “ t_p ” when N_p was recorded. This time interval of $\pm 2 \text{ h}$ is sufficient to cover the entire duration of each burst and to estimate the background level of each burst. To define the burst duration “ Δt_d ”, we identified a continuous time range in which the statistical significance σ_s remained above 1 before and after the peak time t_p . By excluding all count bins in this Δt_d , two-time regions are left in every extracted count history to estimate the background. The background level was determined by fitting count bins in the two time regions with a quadratic function. The background level in Δt_d was then estimated by interpolating the derived quadratic function.

After completing the above analysis, an eye scan was performed to detect any suspicious events that may have been caused by irregular factors such as power failures. As a result of this scan, eight events were identified as suspicious events in the potential burst set. Subsequently, a total of 127 long-duration bursts were selected from the NM data collected between 1998 and 2017. This data set is referred to as the final burst set. None of the events in the final burst set was found to be associated with solar energetic particle events, including ground-level enhancements (Vainio et al. 2017; Cohen and Mewaldt 2018), suggesting that such a solar particle event does not contribute to the production of long-duration bursts.

The current analysis is limited in the detection of faint bursts, because it only considers those with $> 4\sigma$. This selection criterion is one of the reasons for the detection of only 127 events during the long observation period (1998–2017). This frequency is also likely influenced by the higher NM threshold of 7 MeV and the limited spatial illumination of a long-duration burst. Gamma-ray detectors using NaI and BGO scintillators can readily capture long-duration bursts with energies of a few MeV or less (Chilingarian et al. 2019; Wada et al. 2021b), while these low-energy gamma rays are not detectable by the Yangbajing NM. In addition, it is known that a long-duration burst illuminates only a limited area (0.5–1 km) on the ground (Tsuchiya et al. 2011; Wada et al. 2019; Tsurumi et al. 2023). At the altitude of 4300 m, the mean free path of gamma rays with energy of 10–50 MeV is approximately 700–900 m. Therefore, it would be more difficult to clearly detect long-duration bursts originating significantly farther away from NMs than the mean free path.

4 Results and Discussion

4.1 Example of time profiles of long-duration bursts

Figure 2 depicts examples of the 5-minute count histories in the final burst set. It is evident that the individual count histories exhibit significant count increases. Table 1 presents several key characteristics for each of 127 long-duration bursts, including its net count increase denoted as “ N_{tot} ” and the related statistical significance. The N_{tot} is calculated by subtracting the interpolated background from the total observed count in Δt_d . The observed count increases are superimposed on gradual count changes caused primarily by solar diurnal variation, which typically ranges within $\pm 0.3\%$ in amplitude. This variation arises from the anisotropy of galactic cosmic rays below several tens of GeV in interplanetary space.

Unlike the gradual changes induced by the solar diurnal variation, EF variations result in faster changes in the NM count rate. Figure 3 shows examples of the relationship between EF changes and observed count increases. The EF intensity remains at $\sim 0.1 \text{ kV m}^{-1}$ under fair weather conditions, with its sign following atmospheric physics

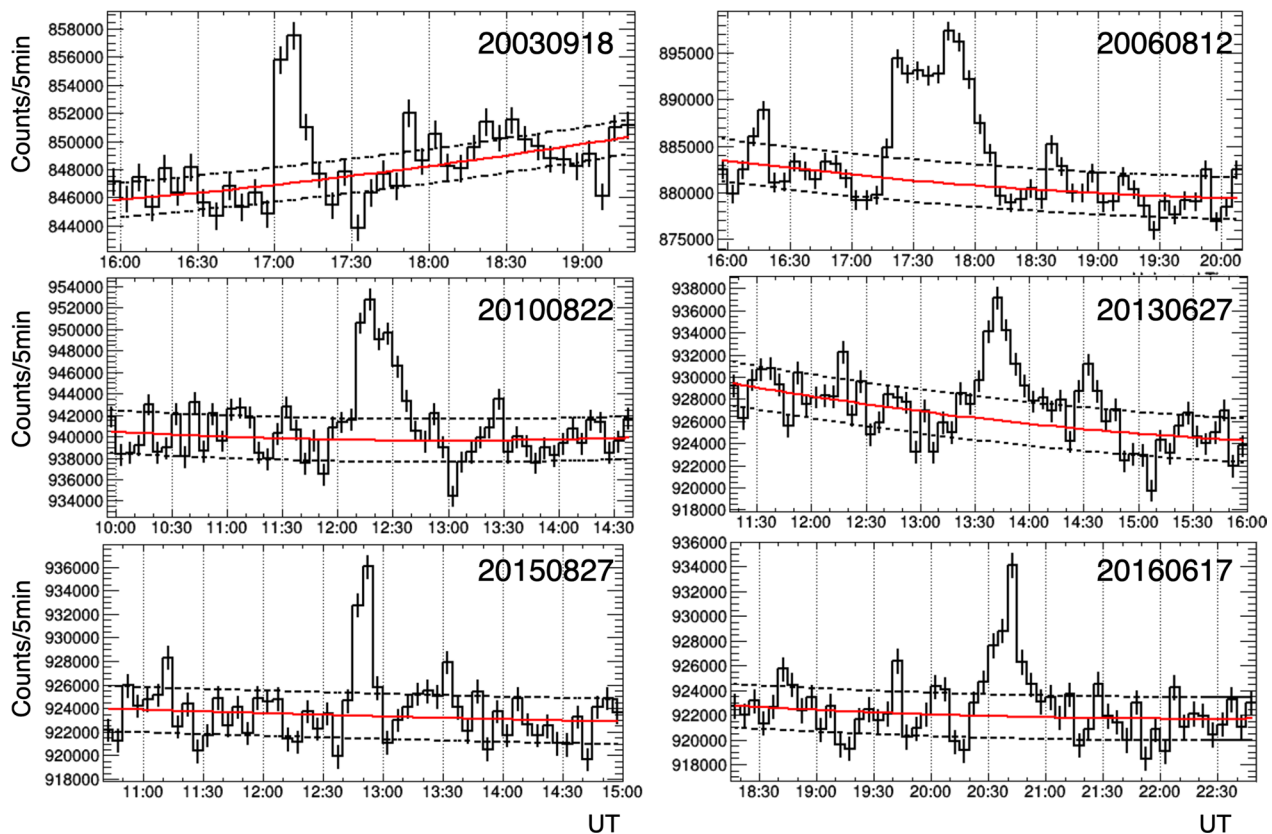


Fig. 2 Examples of the NM count rate histories per 5 min in the final burst set. Each panel is labeled with the date of the event acquisition. The horizontal axis depicts universal time (UT). Each error shown corresponds to a statistical 1σ . Red solid lines represent estimated background levels, while two black dashed lines indicate a range of $\pm \sigma_{\text{day}}$ from the background level

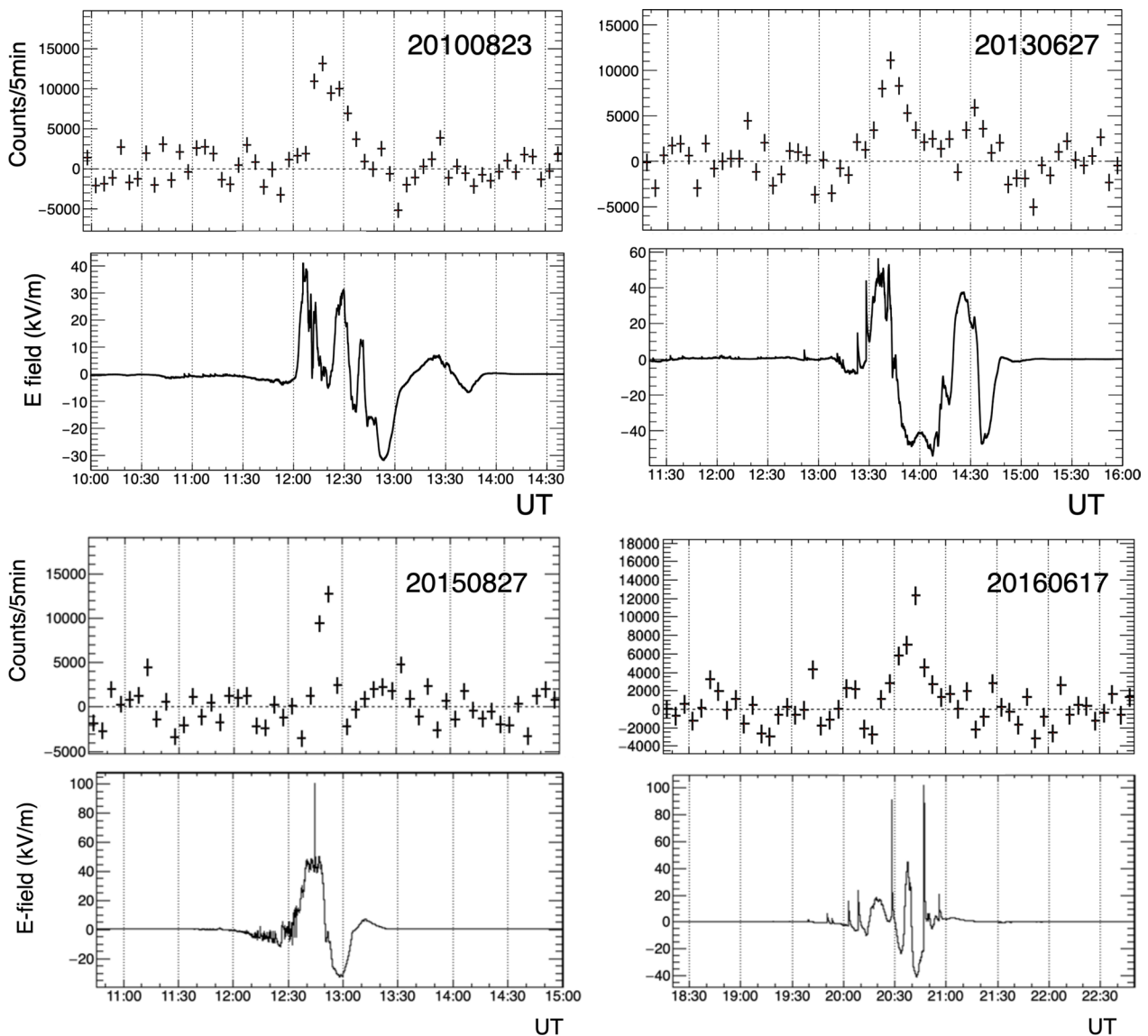


Fig. 3 Comparison between the BG-subtracted NM count rate and electric field (solid line). The abscissa depicts universal time (UT). The errors quoted from the NM counts are statistical 1σ

conventions. A positive value denotes an EF directed downward from the sky to the ground and vice versa. The EF is found to exhibit significant variations lasting for 1–1.5h. While the count increases in the events (Fig. 3) seem to coincide with periods of relatively large positive EFs, the peak times of these count increases do not necessarily align with the peak times of the positive EFs. A possible explanation could be that the alterations in the EF within a thundercloud, responsible for electron acceleration, may not precisely synchronize with the observed variations in the EF at the ground surface. Intense, sharp peaks are also found in EF variations (e.g., 20150827 and 20160617) and indicate the presence of lightning. These

lightning events causing significant peaks in EF variations do not appear to impact the observed long-duration bursts. This is probably because the location of the lightning observed by the EFM is far from NMs. Therefore, when investigating the relationship between EF and long-duration bursts, it would be necessary to specify not only the EF intensity but also the distance to a thundercloud or lightning. This will be our future task.

All other events detected after the EFM installations are also found to have occurred under similar EF conditions (Additional file 1), suggesting a common underlying mechanism to produce a long-duration burst. Typically, a thundercloud is considered to have a tripole

Table 1 The parameters determined for individual events in the final burst set

Date (YYYYMMDD)	t_s (HHMM) ^a (UT)	t_e (HHMM) ^b (UT)	Δt_d (s)	N_{tot}	Significance ^c
19990526	1130	1134	240	24866	15.8
19990609	1430	1455	1500	35669	7.7
19990620	0730	0755	1500	24092	6.9
19990629	1910	1925	900	17985	7.9
19990808	1405	1425	1200	15918	5.1
19990818	1330	1405	2100	32409	6.9
19990830	1300	1340	2400	41992	9.2
19990905	1355	1425	1800	40935	12.0
20000523	1950	2025	2100	39599	10.7
20000527	1040	1050	600	13721	6.5
20000701	1820	1835	900	31168	10.8
20000713	0835	0900	1500	44507	8.4
20000720	1225	1245	1200	25997	8.0
20000729	1450	1515	1500	26050	6.7
20000816	0820	0855	2100	39777	6.9
20000818	1320	1330	600	22382	6.4
20000818	1400	1415	900	14774	5.2
20000822	0800	0820	1200	28867	9.4
20010426	0715	0730	900	19924	8.8
20010609	1700	1735	2100	51037	11.4
20010620	1325	1345	1200	27694	7.2
20010625	1205	1215	600	11387	5.8
20010801	2005	2020	900	26538	10.0
20020518	1410	1420	600	12270	4.4
20020519	1650	1710	1200	14790	5.0
20020529	1550	1600	600	13043	6.0
20020602	2105	2115	600	15976	7.3
20020730	1610	1630	1200	31907	7.8
20030620	1434	1440	360	12416	4.1
20030628	0950	1015	1500	26251	5.8
20030630	1025	1050	1500	32280	7.3
20030709	0540	0550	600	15861	6.3
20030714	1530	1545	900	10919	4.0
20030820	1455	1515	1200	17700	5.6
20030822	1340	1405	1500	19572	6.3
20030822	1430	1445	900	37628	9.4
20030825	1250	1325	2100	46328	11.0
20030918	1700	1715	900	23264	11.0
20040203	1545	1615	1800	29535	8.0
20040609	2240	2250	600	26507	11.1
20040704	2025	2040	900	22875	6.6
20040725	0735	0800	1500	28833	8.6
20040731	1425	1445	1200	20889	4.7
20040803	1625	1645	1200	22040	5.4
20040804	2225	2255	1800	38885	9.0
20040809	1325	1335	600	18530	10.3
20040811	0825	0845	1200	44852	11.4
20040811	1725	1750	1500	26480	7.5

Table 1 (continued)

Date (YYYYMMDD)	t_s (HHMM) ^a (UT)	t_e (HHMM) ^b (UT)	Δt_d (s)	N_{tot}	Significance ^c
20040830	1600	1615	900	13001	5.2
20040901	1535	1555	1200	12259	4.0
20040904	1215	1235	1200	22654	6.6
20050508	1210	1230	1200	16474	5.9
20050605	0450	0510	1200	23276	7.6
20050615	1320	1340	1200	20656	5.5
20050702	1225	1235	600	47259	6.0
20050724	1520	1545	1500	9991	4.2
20050725	1835	1900	1500	29619	6.4
20050807	1410	1425	900	48742	13.2
20050807	1430	1445	900	13820	4.3
20050826	0720	0740	1200	16826	5.6
20050903	1120	1140	1200	22081	7.5
20050917	0710	0720	600	9444	4.3
20060511	1748	1754	360	10765	5.7
20060528	0535	0545	600	15920	7.0
20060627	1235	1250	900	15087	4.1
20060628	0555	0610	900	18245	5.8
20060808	1730	1740	600	23705	11.0
20060812	1715	1810	3300	113029	15.7
20060829	0730	0800	1800	57789	15.0
20060922	0615	0625	600	17815	6.0
20060924	0839	0845	360	9566	5.4
20070701	1840	1900	1200	30533	9.8
20070713	1430	1445	900	22101	7.1
20070722	0615	0630	900	22137	7.8
20070727	1520	1540	1200	20633	5.6
20070824	1150	1200	600	16041	5.5
20070825	1455	1530	2100	86911	15.4
20080515	1525	1545	1200	20732	6.4
20080531	2125	2150	1500	33840	10.7
20080621	1945	1955	600	18923	7.1
20080711	0640	0650	600	14146	4.8
20080714	1225	1240	900	19914	5.9
20080827	1000	1030	1800	42310	8.5
20090628	1230	1240	600	13239	5.1
20090702	1000	1015	900	9734	4.0
20090702	1020	1030	600	19118	6.4
20090719	2200	2220	1200	43259	13.5
20090725	0650	0715	1500	21689	5.8
20090801	0540	0600	1200	15542	4.5
20090802	1355	1420	1500	26839	7.5
20090906	1000	1025	1500	25122	5.8
20100706	1855	1910	900	15802	5.8
20100722	0445	0505	1200	37639	12.0
20100823	1210	1240	1800	54236	11.1
20100919	1420	1440	1200	30433	8.6
20100924	0750	0820	1800	45447	11.8

Table 1 (continued)

Date (YYYYMMDD)	t_s (HHMM) ^a (UT)	t_e (HHMM) ^b (UT)	Δt_d (s)	N_{tot}	Significance ^c
20110710	1310	1345	2100	29362	8.3
20110811	1735	1745	600	26710	8.2
20120711	0605	0625	1200	30299	8.5
20120714	1750	1805	900	21427	6.2
20120803	2010	2025	900	33062	9.6
20120804	1730	1750	1200	23692	7.3
20120911	0550	0615	1500	25331	6.5
20121010	0645	0655	600	19303	6.0
20130627	1330	1400	1800	44102	7.9
20130902	0810	0825	900	20738	8.0
20140703	1025	1040	900	30253	5.8
20140708	0755	0805	600	15058	5.4
20140716	0835	0850	900	16548	5.4
20140720	1355	1405	600	31341	4.8
20140810	0405	0425	1200	27330	5.3
20140810	1900	1915	900	41085	9.8
20140821	1516	1522	360	12142	4.5
20140823	1040	1055	900	30624	6.5
20140911	1435	1455	1200	37654	10.2
20150827	1245	1300	900	19220	5.7
20160617	2025	2055	1800	24536	7.4
20160702	1755	1810	900	32135	8.2
20160704	1435	1510	2100	18502	6.3
20160710	1210	1220	600	41234	7.5
20160717	1220	1255	2100	24763	5.8
20160717	1348	1400	720	39823	8.5
20160801	0700	0720	1200	29004	6.5
20170705	1330	1340	600	17946	6.3
20170816	1305	1340	2100	50353	15.4
20170816	2030	2105	2100	46590	13.2
20170820	0805	0835	1800	58489	11.7

^a Start time^b End time^c Significance of N_{tot}

charge structure, comprising a lower positive charge region (LPCR), a middle negative charge region, and an upper positive charge region (Cooray 2015). Electrons, located between the LPCR and the middle negative charge region, undergo the electric-field acceleration toward the LPCR and emit high-energy photons through bremsstrahlung directed to the ground. Based on measurements taken in the TP at an altitude of 4500 m above sea level (a.s.l.), it was found that the cloud base altitude is generally 1 km above the ground surface (Qie et al. 2005). In our previous study (Tsuchiya et al. 2012), we examined a long-duration burst that occurred on 22

July 2010 (listed as 20100722 in Table 1), and found that about 90% of the NM count enhancement was caused by bremsstrahlung photons emitted by electrons accelerated in thunderclouds. This estimation assumed a cloud base altitude of typically about 1 km above the ground surface. Actually, the constitution ratio of these photons varies according to the distance between the cloud base and the ground, ranging from 85% at a distance of 5 km to 95% at a distance of 0.3 km (Tsuchiya et al. 2012). Therefore, the present bursts exhibit constitution ratios of 85–95% if the cloud-base altitude is in between 0.3 and 5 km.

4.2 Duration

Figure 4 presents the duration distribution for the final burst set. Most of the observed duration ranged between 10 and 40 min, occasionally extending to ~ 60 min. This trend agrees with the typical life cycle of thunderclouds, 30–60 min, during the presummer and summer seasons. Their mature stage, which is likely to produce lightning, generally persists for 15–30 min (Ferrier and Houze 1989).

The ARGO-YBJ experiment, operating ~ 200 m away from the NM location, observed variations of the air-shower rate during 2012 (Axikegu et al. 2022). These variations lasted 14 to 55 min, and are in good agreement with our results. Count enhancements with similar duration have been identified on Mt. Aragats (3250 m a.s.l.) and Mt. Lomnický Štít (2634 m a.s.l.), using multiple detectors such as NMs, a NaI detector, and a plastic scintillation detector. The count increases obtained by NMs (Chilingarian et al. 2010, 2011) lasted ~ 10 min, and most enhancements of the NaI count in energy > 3 MeV lasted for a few minutes to 50 min, with rare occasions extending to 120 min (Chilingarian et al. 2019). Similarly, those obtained at Mt. Lomnický Štít lasted for 1–15 min (Chum et al. 2020). The typical durations within 50 min are in agreement with the present result. However, the > 120 min duration has never been observed at the Yangbajing observatory. This discrepancy in burst duration may be attributed to two factors. One is the different meteorological conditions between Mt. Aragats (3250 m a.s.l.) and Yangbajing (4300 m a.s.l.): for example, successive generations of cells in thunderclouds might be more pronounced on Mt. Aragats. This difference may result in different life cycles for thundercloud-charged layers, where electron acceleration takes place. The other is a difference in the energy threshold for photons of 7 MeV for the Yangbajing NM and 3 MeV for their NaI detector. This difference in energy thresholds could also lead to different duration behaviors.

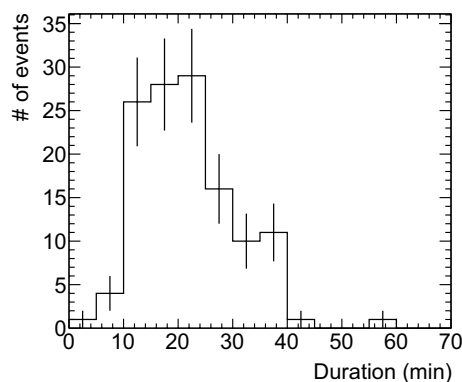


Fig. 4 Duration distribution of long-duration bursts in the final burst set

In contrast to high-altitude observations made during the pre-summer or summer seasons, observations conducted at the Japan Sea in winter seasons have revealed an alternative perspective on long-duration bursts, which generally last only a few minutes (Torii et al. 2002; Tsuchiya et al. 2007a, 2011; Wada et al. 2021b). According to Kitagawa and Michimoto (1994), tripole charge structures become apparent during the mature stages of winter thunderclouds. These tripole structures persist for less than 10 min during early or late winter and for even shorter duration, less than a few minutes during midwinter. Thus, it is reasonable to postulate that differences in the life cycles of thunderclouds are responsible for the noticeable difference in burst duration among long-duration bursts during the summer and winter seasons.

4.3 Diurnal variation

The distribution of the onset times for the final burst set is shown in Fig. 5. This distribution is clearly divided into two sections: one covering the period from 00:00 to 10:00 local time (LT) and the other covering 10:00 to 24:00 LT. LT is calculated as 6 h + universal time (UT), considering the geographical longitude of 90° . In the total number of observed bursts, 11% of them began at 00:00–10:00 LT and the rest occurred at 10:00–24:00 LT. The latter time region contains the period of increased convective activity in convective clouds over the TP as reported by Uyeda et al. (2001) which showed that strong updrafts generated by land surfaces heated due to solar radiation in TP result in the rapid development of convective clouds during 09:00–13:00 LT in the premonsoon seasons and 12:00–16:00 LT in the monsoon seasons. In addition, Qie et al. (2003) investigated lightning activity between 1998 and 2002 in TP using the lightning image sensor onboard the Tropical Rainfall Measuring Mission. Their investigation indicates that 6% and 78% of lightning flashes in the diurnal lightning activity occur in 00:00–10:00 LT and 12:00–19:00 LT, respectively. Therefore, a clear correlation is evident between the distribution of the observed burst start times and the temporal pattern of lightning flashes.

Wada et al. (2021b) examined the onset time distribution of 70 long-duration bursts detected in the coastal area of the Japan Sea over 4 winter seasons from 2015 to 2018. They divided the data into two parts: the daytime spanning 06:00–18:00 LT and the nighttime encompassing the remaining time period. They showed that the number of events in daytime is 15 and significantly smaller than 55, the number of events in nighttime. The present study also shows a comparable trend, indicating that the number of events during the day, 43, is less than the number of events during the night, 84, with a

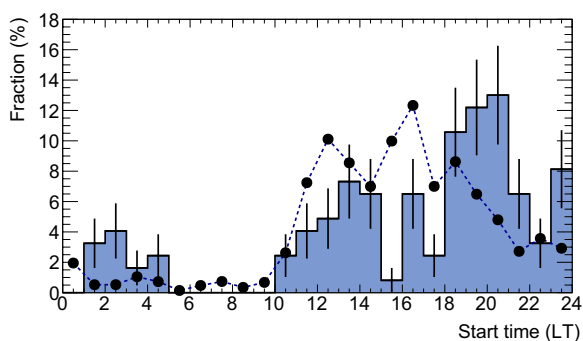


Fig. 5 Start time distribution of events in the final burst set (filled histogram), plotted as a function of local time (LT) computed by 6 h + UT. The filled circles represent the diurnal variation of lightning activity in TP in 1998–2002 (Qie et al. 2003)

statistical significance of 3.6σ . This trend is supported to some extent by observations at Mt. Aragats (Chilingarian et al. 2019). These results suggest that long-duration bursts of high-energy radiation are likely to occur during local nighttime hours. The nighttime phase corresponds to the dissipation phase of thunderclouds, during which the occurrence of strong electric fields capable of causing relativistic runaway electron avalanches is less likely. Therefore, it is plausible that the long-duration bursts observed at night could be attributed to the process of Modification Of Spectra as discussed by Chilingarian et al. (2014) and Diniz et al. (2022).

4.4 Seasonal variation

Figure 6 shows the seasonal variation in the occurrences number of the final burst set. Among them, 122 events (97% of the total 127 events) were observed between May and September, corresponding to the premonsoon and monsoon seasons in TP. The seasonal trend obtained

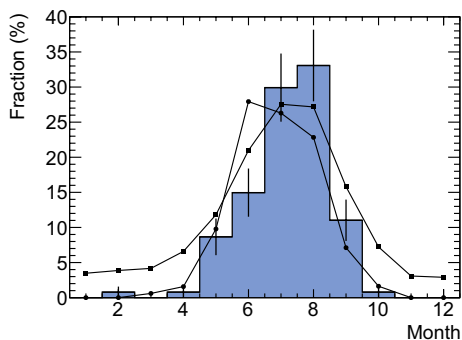


Fig. 6 Distribution of months in which events occurred in the final burst set (filled histogram). Filled squares and circles indicate lightning activity and precipitation, respectively, during the years 1998–2002 in the central part of the TP (Qie et al. 2003)

is similar to that of precipitation and lightning activity within the TP region (Qie et al. 2003). This similarity suggests that long-duration bursts tend to occur during the rainy season when lightning is more frequent, as expected.

According to the EF measurements from March 2010 to February 2012 (Amenomori et al. 2013), the total number of thundercloud occurrences at Yangbajing was 158 days. During this period, the Yangbajing NM detected only seven long-duration bursts (Table 1). Interestingly, Amenomori et al. (2013) showed that thunderclouds were also observed in 54 days during winter seasons from December to March. However, the Yangbajing NM did not detect any long-duration bursts during this winter period, except only one recorded between 1998 and 2017 (20040203 in Table 1). This infrequent detection during winter suggests that the EF intensity due to thunderclouds may not be the sole factor governing the production of long-duration bursts.

The ARGO-YBJ experiment, conducted near the NM location, detected twenty count enhancements during thunderstorms in 2012 between April and October (Axikegu et al. 2022). This period coincides with the present result. Notably, four (20120714, 20120804, 20120911, and 20121010) of the six long-duration bursts detected in 2012 (Table 1) align with the dates recorded by the ARGO-YBJ experiment. The effective area of the Yangbajing NM (32 m^2) is smaller than that of the ARGO-YBJ detector ($\sim 110 \times 100 \text{ m}^2$). A larger effective area is likely to detect more long-duration bursts with narrow illumination areas. Hence, the difference in effective area is considered one of the main factors contributing to the variation in the number of events detected in 2012 (6 for the Yangbajing NM and 20 for the ARGO-YBJ experiment).

Muraki et al. (2004) studied a seasonal variation using a large-area meson monitor installed at Mt. Norikura (2770 m a.s.l.) in Japan. The meson monitor comprises scintillation detectors, and primarily detects charged particles but also has some sensitivity to neutral particles such as neutrons and gamma rays. Analyzing data obtained from October 1990 to January 2002, they found that the derived seasonal variation matches the pattern of thunderstorm occurrence. The seasonal variation observed with the Yangbajing NM is similar to their result. This is probably because the two areas are influenced by the Asian monsoon. Chilingarian et al. (2019) also showed a seasonal variation, with a notable peak in May, which may probably be due to different meteorological conditions compared to those observed in the TP and at Mt. Norikura.

4.5 Annual variation

In Fig. 7, we present an annual variation in occurrences numbers of the final burst set (red histogram in the top panel) and compare it with the annual variations of the sunspot number (black histogram in the top panel) and the galactic cosmic-ray intensity (histogram in the bottom panel) to explore their possible correlations with long-duration bursts. The sunspot number data were sourced from Sunspot Index and Long-term Solar Observations: <https://www.sidc.be/silso/home>. For our investigation, we used Jungfraujoch NM data that are available from the World Data Centre for Cosmic Rays (<https://cidas.isee.nagoya-u.ac.jp/WDCCR>), but annual variations of galactic cosmic-ray intensity are almost common in all NM data. It has been hypothesized that galactic cosmic rays play a role in the induction of thunderstorm-related events by providing seed electrons (Gurevich

et al. 1992; Babich et al. 2007; Carlson et al. 2008; Gurevich and Karashtin 2013). As is well known, variations in sunspot number reflect solar activity that has the 11-year cycle, and is inversely correlated with variations of galactic cosmic-ray intensity at Earth. Thus, it is natural to conjecture that solar activity may influence the occurrence of long-duration bursts.

To quantify the annual variation of the occurrence rate in the final burst set, we employed the following functions for fitting: (1) a constant function, (2) a linear function, and (3) a periodic function. Functions (1) and (2) are denoted $f_c(t) = a_0$ and $f_l(t) = a_0 + a_1t$, respectively. Here, a_0 and a_1 represent a constant and a slope, respectively. The variable t shows the elapsed year since 1998. The function (1) assumes that solar activity or cosmic rays exert time-independent effects on the observed number of long-duration bursts. Function (2) assumes a

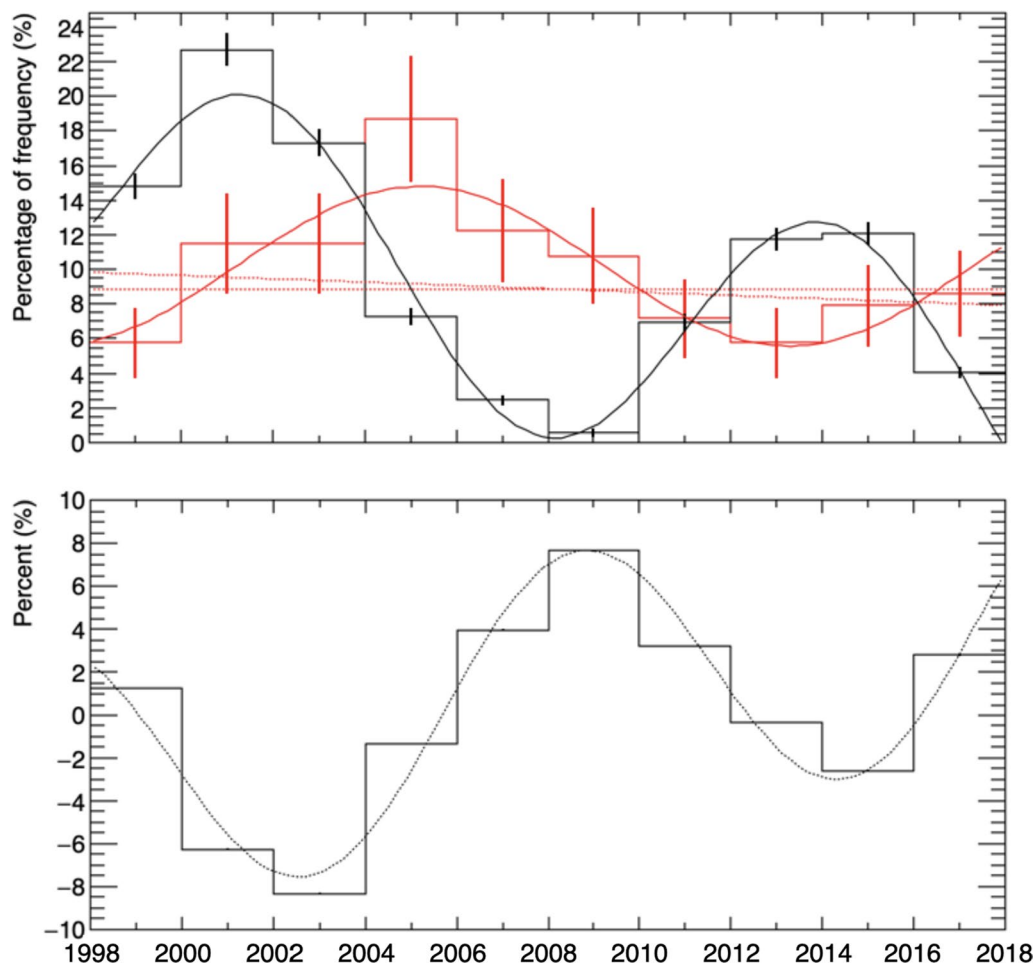


Fig. 7 Top: annual occurrence variation of the final data set (red histogram). The black histogram shows an annual variation in sunspot number expressed in %. Solid red and black curves denote a periodic function of $f_p(t)$ and $f_{sun}(t)$, respectively, while dashed lines represent $f_c(t)$ and $f_l(t)$. The error bar represents statistical 1σ . Bottom: the annual variation of cosmic-ray flux measured by neutron monitors located at Jungfraujoch. The NM data were obtained from the following <https://cidas.isee.nagoya-u.ac.jp/WDCCR/index.html>

Table 2 The fitting parameters determined for each function

	A	T	ϕ	a_0	a_1	χ^2/ν^a
Function	(%)	(yr)	(rad)	(yr)	($\times 10^{-1}\%$ /yr)	
$f_c(t)$	–	–	–	$(8.8 \pm 0.8) \times 10^{-2}$	–	16/9
$f_l(t)$	–	–	–	$(1.0 \pm 0.2) \times 10^{-1}$	-1.5 ± 1.4	14/8
$f_p(t)$	4.6 ± 1.3	16.4 ± 1.7	-1.1 ± 0.4	0.100 ± 0.009	–	3.9/6
$f_{\text{sun}}(t)$	8.0 ± 0.2	12.57 ± 0.13	-0.22 ± 0.06	0.141 ± 0.004	-5.8 ± 0.3	33/5
$f_{\text{cr}}(t)$	6.422 ± 0.009	11.772 ± 0.005	2.174 ± 0.002	-2.920 ± 0.013	0.388 ± 0.001	50/5

^a ν is degree of freedom.

descending (or ascending) trend during the 1998–2017 period, based on the fact that the peak sunspot number was smaller around 2013–2015 than during the period around 2000–2002. The last periodic function (3) is expressed as

$$f_p(t) = a_0 + A \sin\left(\frac{2\pi}{T}t + \phi\right), \quad (2)$$

where A , T and ϕ denote a normalization constant, a period, and a phase, respectively. As listed in Table 2, the resultant χ^2/ν values (ν is the degree of freedom) indicate that $f_p(t)$ provides the best fit to reproduce the derived annual variation of the final burst set. This result implies the potential presence of periodicity in the annual occurrence rate of the observed long-duration bursts.

For comparison, we evaluated periods of annual variations in the sunspot number and cosmic-ray flux as well by fitting the following function to the variations

$$f_{\text{sun,cr}}(t) = a_0 + a_1 t + A \sin\left(\frac{2\pi}{T}t + \phi\right). \quad (3)$$

This function considers a clear decrease (increase) in the amplitude of the sunspot number variation (cosmic-ray flux) over the years. The resulting curves of $f_{\text{sun}}(t)$ and $f_{\text{cr}}(t)$ are drawn in Fig. 7, and the parameters determined are listed in Table 2. The evaluated periods (T) for the sunspot number and cosmic-ray flux deviate from the period estimated from the final burst set by 2.2σ and 2.7σ (Table 2). In addition, by using the derived periods (T) and phases (ϕ) in Table 2, we can calculate the peak years of f_p and f_{sun} , and the year of the minimum of f_{cr} , each measured from 1998, as 6.9 ± 1.3 years, 3.58 ± 0.13 years, and 4.756 ± 0.003 years, respectively. From these values, possible slight lags of f_p with respect to f_{sun} and f_{cr} were estimated as 3.3 ± 1.3 years and 2.1 ± 1.3 years, respectively. While the present analysis suggests a potential connection between long-duration bursts and solar activity or cosmic rays, we need more data over a longer

time period before definitively confirming the periodicity and delay.

5 Conclusions

Long-duration bursts were detected by the Yangbajing NM located at 4300 m a.s.l. during the period of 1998–2017. The detected bursts have a typical duration of 10 to 40 min. This duration distribution suggests that electrons undergo continuous acceleration to 10 MeV or higher within a few tens of minutes. In the coastal area of the Japan Sea, long-duration bursts have also been observed in winter seasons and typically last for a few minutes. The difference in duration would result from the distinct life cycles of winter and summer thunderclouds.

The seasonal and diurnal variations in the occurrence number of long-duration bursts agreed well with those variations of lightning and precipitation on the TP. This agreement justifies the selection and subsequent analysis of the Yangbajing NM data. The present work, based on 19-year data, suggests the possibility that the annual variation of long-duration bursts has a periodicity of ~ 16 years and a lag of ~ 3 years relative to solar activity. To gain further insight into the observed annual variability, it would be necessary to conduct longer-term high-energy radiation observations coupled with comprehensive meteorological measurements.

The present work highlights the importance of NM data for understanding the temporal variability and underlying production mechanisms of long-duration bursts of high-energy radiation associated with thunderclouds. Since the 1950s, numerous NMs have been operational at various observatories around the world (Bütikofer 2018). These NM data would allow us to unravel the real connections between long-duration bursts, cosmic rays, and solar activity.

Abbreviations

TP	Tibetan plateau
NM	Neutron monitor
EFM	Electric field mill

Supplementary Information

The online version contains supplementary material available at <https://doi.org/10.1186/s40645-024-00625-y>.

Additional File 1. This file includes comparisons between long-duration bursts detected in 2010–2017 (Table 1 in the main text) and EF variations, but not include the comparisons presented in the main text. Due to periods of the EFM shutdown, EF variations could not be obtained for all periods of 2010–2017.

Acknowledgements

We sincerely thank Prof. T. Shinoda (Nagoya Univ.) for giving information on meteorological conditions on the Tibetan plateau.

Author contributions

HT, KH, and KK were responsible for data analysis, interpretation, and the proposed writing of this paper. KH and KK installed the EFMs and performed their maintenance. HT, KM, CK, MO, MT, SS, QS, SW, CH, and LZ contributed to the maintenance of the Yangbajing NM. All authors read and approved the final manuscript.

Funding

This work was partly supported by JSPS KAKENHI Grant Number 21H01116.

Availability of data and materials

The datasets used and/or analyzed during the current study are available from the corresponding author on reasonable request.

Declarations

Competing interests

The authors declare that they have no conflict of interest.

Received: 6 December 2023 Accepted: 7 April 2024

Published online: 03 May 2024

References

- Amenomori M, Bi XJ, Chen D, Chen TL, Chen WY, Cui SW, Ding LK, Feng CF, Feng Zhaoyang, Feng ZY, Gou QB, Guo YQ, He HH, He ZT, Hibino K, Hotta N, Hu Haibing, Hu HB, Huang J, Jia HY, Jiang L, Kajino F, Kasahara K, Katayose Y, Kato C, Kawata K, Kozai M, Le GM, Li AF, Li HJ, Li WJ, Liu C, Liu JS, Liu MY, Lu H, Meng XR, Mizutani K, Munakata K, Nanjo H, Nishizawa M, Ohnishi M, Ohta I, Ozawa S, Qian XL, Qu XB, Saito T, Saito TY, Sakata M, Sako TK, Shao J, Shibata M, Shiomi A, Shirai T, Sugimoto H, Takita M, Tan YH, Tateyama N, Torii S, Tsuchiya H, Udo S, Wang H, Wu HR, Xue L, Yamamoto Y, Yang Z, Yasue S, Yuan AF, Yuda T, Zhai LM, Zhang HM, Zhang JL, Zhang XY, Zhang Y, Zhang Y, Zhang Y, Zhou XX (2013) Observation of thundercloud-related charged particles in Tibet. In: Proceedings of 33rd international cosmic ray conference, pp 3524–3527
- Babich LP, Bochkov EI, Donskoi EN, Kutsyk IM (2010) Source of prolonged bursts of high-energy gamma rays detected in thunderstorm atmosphere in Japan at the coastal area of the Sea of Japan and on high mountaintop. *J Geophys Res Space Phys.* <https://doi.org/10.1029/2009JG015017>
- Babich LP, Donskoy EN, Il'kaev RI, Kutsyk IM, Roussel-Dupré RA (2004) Fundamental parameters of a relativistic runaway electron avalanche in air. *Plasma Phys Rep* 30(7):616–624. <https://doi.org/10.1134/1.1778437>
- Babich LP, Donskoy EN, Roussel-Dupré RA (2007) Study of relativistic electron avalanche enhancement in the atmosphere at low overvoltages due to avalanche bremsstrahlung. *Geomagn Aeron* 47(4):515–524. <https://doi.org/10.1134/S0016793207040135>
- Axikegu BB, Bernardini P, Bi XJ, Cao Z, Catalanotti S, Chen SZ, Chen TL, Cui SW, Dai BZ, D'Amone A, Danzengluobu De Mitri I, D'Ettoire Piazzoli BD, Di Girolamo T, Di Sciascio G, Feng CF, Feng Z, Gao W, Gou QB, Guo YQ, He HH, Hu H, Hu H, Iacovacci M, Iuppa R, Jia HY, Labaciren Li HJ, Liu C, Liu J, Liu MY, Lu H, Ma LL, Ma XH, Mancarella G, Mari SM, Marsella G, Mastroianni S, Montini P, Ning CC, Perrone L, Pistilli P, Salvini P, Santonico R, Shen PR, Sheng XD, Shi F, Surdo A, Tan YH, Vallania P, Vernetto S, Vigorito C, Wang H, Wu CY, Wu HR, Xue L, Yang QY, Yang XC, Yao ZG, Yuan AF, Zha M, Zhang HM, Zhang L, Zhang XY, Zhang Y, Zhao J, Zhaxisangzhu Z, Zhou XX, Zhu FR, Zhu QQ (2022) Cosmic ray shower rate variations detected by the ARGO-YBJ experiment during thunderstorms. *Phys Rev D* 106:022008
- Bütikofer R (2018) Ground-based measurements of energetic particles by neutron monitors. In: Malandraki OE, Crosby NB (eds) *Solar particle radiation storms forecasting and analysis*, vol 444. Springer International Publishing, Cham, pp 95–111. https://doi.org/10.1007/978-3-319-60051-2_6
- Carlson BE, Lehtinen NG, Inan US (2008) Runaway relativistic electron avalanche seeding in the Earth's atmosphere. *J Geophys Res Space Phys* 113(A10):1–5. <https://doi.org/10.1029/2008JA013210>
- Chilingarian A, Daryan A, Arakelyan K, Hovhannisyann A, Mailyan B, Melkumyan L, Hovsepyan G, Chilingaryan S, Reymers A, Vanyan L (2010) Ground-based observations of thunderstorm-correlated fluxes of high-energy electrons, gamma rays, and neutrons. *Phys Rev D.* <https://doi.org/10.1103/PhysRevD.82.043009>
- Chilingarian A, Hovsepyan G, Hovhannisyann A (2011) Particle bursts from thunderclouds: Natural particle accelerators above our heads. *Phys Rev D* 83(6):96. <https://doi.org/10.1103/PhysRevD.83.062001>
- Chilingarian A, Hovsepyan G, Vanyan L (2014) On the origin of the particle fluxes from the thunderclouds: energy spectra analysis. *Europhys Lett* 106(5):59001. <https://doi.org/10.1209/0295-5075/106/59001>
- Chilingarian A, Mkrtchyan H, Karapetyan G, Chilingaryan S, Sargsyan B, Arestakesyan A (2019) Catalog of 2017 thunderstorm ground enhancement (TGE) events observed on Aragats. *Sci Rep* 9(1):6253. <https://doi.org/10.1038/s41598-019-42786-7>
- Chum J, Langer R, Baše J, Kollárik M, Strhárský I, Diendorfer G, Rusz J (2020) Significant enhancements of secondary cosmic rays and electric field at the high mountain peak of Lomnický štít in High Tatras during thunderstorms. *Earth Planets Space* 72(1):28. <https://doi.org/10.1186/s40623-020-01155-9>
- Clem JM, Dorman LI (2000) Neutron monitor response functions. *Space Sci Rev* 93:335–359. <https://doi.org/10.1023/A:1026508915269>
- Cohen CMS, Mewaldt RA (2018) The ground-level enhancement event of September 2017 and other large solar energetic particle events of cycle 24. *Space Weather* 16(10):1616–1623. <https://doi.org/10.1029/2018SW002006>
- Cooray V (2015) *Charge generation in thunderclouds and different forms of lightning flashes*. Springer, Berlin
- Diniz G, Wada Y, Ohira Y, Nakazawa K, Enoto T (2022) Atmospheric electron spatial range extended by thundercloud electric field below the relativistic runaway electron avalanche threshold. *J Geophys Res Atmos* 127(3):e2021JD035958. <https://doi.org/10.1029/2021JD035958>
- Dwyer JR (2003) A fundamental limit on electric fields in air. *Geophys Res Lett.* <https://doi.org/10.1029/2003GL017781>
- Dwyer JR (2007) Relativistic breakdown in planetary atmospheres. *Phys Plasmas.* <https://doi.org/10.1063/1.2709652>
- Dwyer JR, Smith DM, Cummer SA (2012) High-energy atmospheric physics: terrestrial gamma-ray flashes and related phenomena. *Space Sci Rev* 173(1–4):133–196. <https://doi.org/10.1007/s11214-012-9894-0>
- Enoto T, Wada Y, Furuta Y, Nakazawa K, Yuasa T, Okuda K, Makishima K, Sato M, Sato Y, Nakano T, Umemoto D, Tsuchiya H (2017) Photonuclear reactions triggered by lightning discharge. *Nature* 551(7681):481–484. <https://doi.org/10.1038/nature24630>
- Ferrier BS, Houze RA (1989) One-dimensional time-dependent modeling of gate cumulonimbus convection. *J. Atmos. Sci.* 46:330–352. [https://doi.org/10.1175/1520-0469\(1989\)046<0330:ODTDMO>2.0.CO;2](https://doi.org/10.1175/1520-0469(1989)046<0330:ODTDMO>2.0.CO;2)
- Gurevich AV, Karashtin AN (2013) Runaway Breakdown and Hydrometeors in Lightning Initiation. *Phys Rev Lett.* <https://doi.org/10.1103/PhysRevLett.110.185005>
- Gurevich AV, Milikh GM, Roussel-Dupré R (1992) Runaway electron mechanism of air breakdown and preconditioning during a thunderstorm. *Phys Lett A* 165(5–6):463–468. [https://doi.org/10.1016/0375-9601\(92\)90348-P](https://doi.org/10.1016/0375-9601(92)90348-P)
- International Atomic Energy Agency (2000) *Handbook on photonuclear data for applications cross-sections and spectra*. IAEA-TECDOC-11178, IAEA, Vienna. <https://www.iaea.org/publications/6043/handbook-on-photonuclear-data-for-applications-cross-sections-and-spectra>

- Kitagawa N, Michimoto M (1994) Meteorological and electrical aspects of winter thunderclouds. *J Geophys Res Atmos* 99(D5):10713–10721. <https://doi.org/10.1029/94JD00288>
- Kochkin P, Sarria D, Lehtinen N, Mezentsev A, Yang S, Genov G, Ullaland K, Marisaldi M, Østgaard N, Christian HJ, Grove JE, Quick M, Al-Nussirat S, Wulf E (2021) A rapid gamma-ray glow flux reduction observed from 20 km altitude. *J Geophys Res Atmos* 126(9):200. <https://doi.org/10.1029/2020JD033467>
- Miyasaka H, Takahashi E, Shimoda S, Yamada Y, Kondo I, Tsuchiya H, Makishima K, Zhu FR, Tan YH, Hu HB, Tang YQ, Clem J (2005) The Solar Event on 20 January 2005 observed with the Tibet YBJ Neutron monitor observatory. In: Proceedings of 29th international cosmic ray conference, pp 241–244
- Muraki Y, Axford WJ, Matsubara Y, Masuda K, Miyamoto Y, Menjou H, Sakakibara S, Sako T, Takami T, Yamada T, Shibata S, Munakata Y, Munakata K, Yasue S, Sakai T, Mitsui K, Fujimoto K, Flückiger E (2004) Effects of atmospheric electric fields on cosmic rays. *Phys Rev D*. <https://doi.org/10.1103/PhysRevD.69.123010>
- Østgaard N, Christian HJ, Grove JE, Sarria D, Mezentsev A, Kochkin P, Lehtinen N, Quick M, Al-Nussirat S, Wulf E, Genov G, Ullaland K, Marisaldi M, Yang S, Blakeslee RJ (2019) Gamma ray glow observations at 20-km altitude. *J Geophys Res Atmos* 124(13):7236–7254. <https://doi.org/10.1029/2019JD030312>
- Qie XS, Toumi R, Yuan T (2003) Lightning activities on the Tibetan Plateau as observed by the lightning imaging sensor. *J Geophys Res* 108(D17):4551. <https://doi.org/10.1029/2002JD003304>
- Qie XS, Zhang TL, Chen CG, Zhang GS, Zhang T, Wei WZ (2005) The lower positive charge center and its effect on lightning discharges on the Tibetan Plateau. *Geophys Res Lett*. <https://doi.org/10.1029/2004GL022162>
- Torii T, Sugita T, Tanabe S, Kimura Y, Kamogawa M, Yajima K, Yasuda H (2009) Gradual increase of energetic radiation associated with thunderstorm activity at the top of Mt. Fuji. *Geophys Res Lett*. <https://doi.org/10.1029/2008GL037105>
- Torii T, Takeishi M, Hosono T (2002) Observation of gamma-ray dose increase associated with winter thunderstorm and lightning activity. *J Geophys Res Atmos*. <https://doi.org/10.1029/2001JD000938>
- Tsuchiya H, Enoto T, Torii T, Nakazawa K, Yuasa T, Torii S, Fukuyama T, Yamaguchi T, Kato H, Okano M, Takita M, Makishima K (2009) Observation of an energetic radiation burst from mountain-top thunderclouds. *Phys Rev Lett* 102(25):255003. <https://doi.org/10.1103/PhysRevLett.102.2550>
- Tsuchiya H, Enoto T, Yamada S, Yuasa T, Kawaharada M, Kitaguchi T, Kokubun M, Kato H, Okano M, Nakamura S, Makishima K (2007) Detection of high-energy gamma rays from winter thunderclouds. *Phys Rev Lett*. <https://doi.org/10.1103/PhysRevLett.99.165002>
- Tsuchiya H, Enoto T, Yamada S, Yuasa T, Nakazawa K, Kitaguchi T, Kawaharada M, Kokubun M, Kato H, Okano M, Makishima K (2011) Long-duration γ ray emissions from 2007 and 2008 winter thunderstorms. *J Geophys Res*. <https://doi.org/10.1029/2010JD015161>
- Tsuchiya H, Hibino K, Kawata K, Hotta N, Tateyama N, Ohnishi M, Takita M, Chen D, Huang J, Miyasaka M, Kondo I, Takahashi E, Shimoda S, Yamada Y, Lu H, Zhang JL, Yu XX, Tan YH, Nie SM, Munakata K, Enoto T, Makishima K (2012) Observation of thundercloud-related gamma rays and neutrons in Tibet. *Phys Rev D* 85(9):1–14. <https://doi.org/10.1103/PhysRevD.85.092006>
- Tsuchiya H, Miyasaka H, Takahashi E, Shimoda S, Yamada Y, Kondo I, Makishima K, Zhu F, Tan Y, Hu H, Tang Y, Zhang J, Lu H, Meng X (2007) Upper limits on the solar-neutron flux at the Yangbajing neutron monitor from BATSE-detected solar flares. *Astron Astrophys* 468(3):1089–1097. <https://doi.org/10.1051/0004-6361:20066680>
- Tsurumi M, Enoto T, Ikkatai Y, Wu T, Wang D, Shinoda T, Nakazawa K, Tsuji N, Diniz GS, Kataoka J, Koshikawa N, Iwashita R, Kamogawa M, Takagaki T, Miyake S, Tomioka D, Morimoto T, Nakamura Y, Tsuchiya H (2023) Citizen science observation of a gamma-ray glow associated with the initiation of a lightning flash. *Geophys Res Lett* 50(13):e2023GL103612. <https://doi.org/10.1029/2023GL103612>
- Uyeda H, Yamada H, Horikomi J, Shirooka R, Shimizu R, Liping L, Ueno K, Fujii H, Koike T (2001) Characteristics of convective clouds observed by a Doppler radar at Naqu on Tibetan Plateau during the GAME-Tibet IOP. *J Meteorol Soc Jpn* 79:463–474. <https://doi.org/10.2151/jmsj.79.463>
- Vainio R, Raukunen O, Tylka AJ, Dietrich WF, Afanasiev A (2017) Why is solar cycle 24 an inefficient producer of high-energy particle events? *Astron Astrophys* 604(A47):1–9. <https://doi.org/10.1051/0004-6361/201730547>
- Wada Y, Enoto T, Kubo M, Nakazawa K, Shinoda T, Yonetoku D, Sawano T, Yuasa T, Ushio T, Sato Y, Diniz GS, Tsuchiya H (2021) Meteorological aspects of gamma-ray glows in winter thunderstorms. *Geophys Res Lett* 48(7):e2020GL091910. <https://doi.org/10.1029/2020GL091910>
- Wada Y, Enoto T, Nakamura Y, Furuta Y, Yuasa T, Nakazawa K, Morimoto T, Sato M, Matsumoto T, Yonetoku D, Sawano T, Sakai H, Kamogawa M, Ushio T, Makishima K, Tsuchiya H (2019) Gamma-ray glow preceding downward terrestrial gamma-ray flash. *Commun Phys* 2(1):67. <https://doi.org/10.1038/s42005-019-0168-y>
- Wada Y, Matsumoto T, Enoto T, Nakazawa K, Yuasa T, Furuta Y, Yonetoku D, Sawano T, Okada G, Nanto H, Hisadomi S, Tsuji Y, Diniz GS, Makishima K, Tsuchiya H (2021) Catalog of gamma-ray glows during four winter seasons in Japan. *Phys Rev Res* 3(4):043117. <https://doi.org/10.1103/PhysRevResearch.3.043117>
- Wilson CTR (1924) The electric field of a thundercloud and some of its effects. *Proc Phys Soc Lond* 37(1):32D–37D. <https://doi.org/10.1088/1478-7814/37/1/314>
- Wilson CTR (1925) The acceleration of β -particles in strong electric fields such as those of thunderclouds. *Math Proc Camb Philos Soc* 22(4):534–538. <https://doi.org/10.1017/S0305004100003236>

Publisher's Note

Springer Nature remains neutral with regard to jurisdictional claims in published maps and institutional affiliations.